

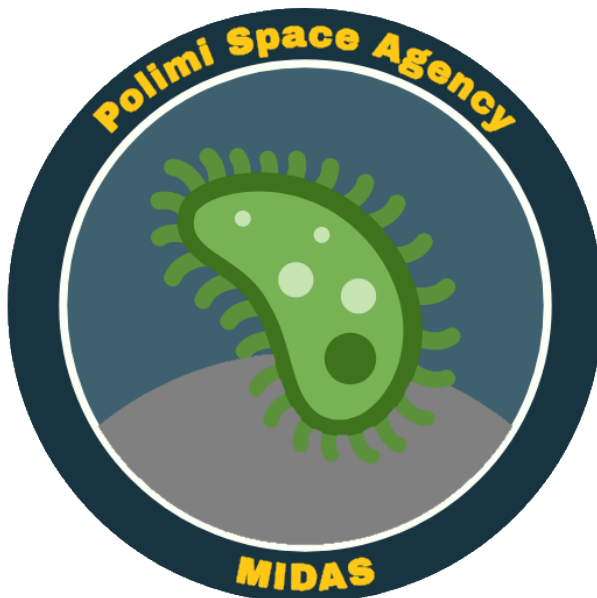


POLITECNICO MILANO 1863

SPACE SYSTEMS ENGINEERING AND OPERATIONS

MIDAS MISSION

GROUP 11



Bardazzi, Niccolò	PC: 10800456, MN: 963039
Carcano, Stefano	PC: 10578334, MN: 975976
Domaschio, Jacopo	PC: 10530480, MN: 968568
Capocchiano, Luca	PC: 10577885, MN: 976231

MSc in Space Engineering - AY 2020/2021

Contents

1	Mission Goals and Expected Results	4
1.1	Mission definition	4
1.2	Primary objective and returns	4
1.3	Ancillary objectives and returns	4
2	Environment	6
3	Mission architecture	8
3.1	Preliminary architecture selected	8
3.2	Trajectory	9
3.3	Conceptual operations	10
3.3.1	Launch	10
3.3.2	Detumbling and cruise mode	11
3.3.3	Mars Gravity Assist	11
3.3.4	Arrival and stand-by mode	13
3.3.5	Observation on Orbit and Touch and Go procedure	15
3.3.6	Experiment and Telecommunication	16
3.3.7	End of Life	17
4	Sensors and Payloads	18
4.1	Bacteria selection	18
4.2	Bioreactor & Methane detector	18
4.2.1	Bioreactor	19
4.2.2	Methane detector	19
4.3	VIS-NIR Camera	20
4.4	LIDAR	21
4.5	Accelerometer and gyroscope	22
4.6	TAGSAM	23

5 Subsystems	25
5.1 Propulsion Subsystem	25
5.1.1 Mass breakdown	26
5.2 Electrical Power Subsystem	27
5.2.1 Power breakdown	27
5.2.2 Solar Arrays	28
5.2.3 Batteries	29
5.3 Thermal Control Subsystem	30
5.4 Telecommunication Subsystem	31
5.4.1 Antenna	33
5.5 Attitude Determination and Control Subsystem	33
6 Configuration	35
7 Conclusions	37
Appendix	39
Bibliography	43

Abstract

Biotechnological resource extraction processes such as biomining and biogas production have the potential to ensure the future of human spacefaring capabilities. These processes have a proven track record on Earth where they fill increasing shares of the market extending from the copper industry to natural gas production. Nowadays space missions rely on predetermined fuel reserves, which are carefully optimised to maximise payload and are still the most driving parameter behind all missions. The implementation of in-situ fuel and material harvesting technologies is fundamental for large scale missions where resupply from Earth would be unsustainable or impossible altogether. Biotechnological processes are less power hungry than other extraction methods, such as optical mining, and could be the ideal solution for resource acquisition in deep-space. While biomining and methanogenic reactions are well established on Earth, the effects on these processes in outer space are unknown. Therefore the objective of this work is to propose a mission aimed at testing the applicability of methanogenic processes in deep-space.

CHAPTER 1

Mission Goals and Expected Results

1.1 Mission definition

The goal of the MIDAS mission is to verify the applicability of biomining techniques in the severe deep-space environment. More specifically the mission focuses on the production of methane and aims to better comprehend the efficiency of the extraction process and the interaction between the microbes and the minerals in deep-space. It is important to test these technologies in deep-space because, if properly developed, that's the environment where they might be more relevant in the future, particularly for their high efficiency, low weight and low power required. The mission will be performed by an autonomous small spacecraft, with an envelope of less than 24 U.

Since carbonaceous chondrite is the key element to be fermented by methanogens anaerobic bacteria, the target for this experiment must be a C-type asteroid. The target chosen for the mission is the asteroid 253 Mathilde, located in the Main Asteroid Belt, which shows a very high carbon content from ground observations. Although some information about Mathilde is known thanks to the fly-by of the NEAR mission in 1997, which gathered an estimation of its gravity field and several pictures, the asteroid is scientifically interesting because there is still uncertainty about its structure and a complete surface mapping does not exist.

1.2 Primary objective and returns

The primary objective of the mission is to acquire a sample of carbonaceous material from the asteroid's surface, to ferment it using a methanogens bacteria culture inside a small bioreactor on board of the s/c and to detect if and how much methane is produced. The expected return is the measurement of the concentration of methane inside the bioreactor through a dedicated optical sensor over time. The detection of at least a few parts per million of methane (enough to be reliably detected by the sensor) will be the threshold for the experiment to be considered successful. Production data will be compared with a control sample on Earth to evaluate how the environment impacts the efficiency.

1.3 Ancillary objectives and returns

The s/c will be equipped with a multispectral camera for navigation and to select the best spot of the asteroid to acquire the desired sample. The same camera will be used while on orbit

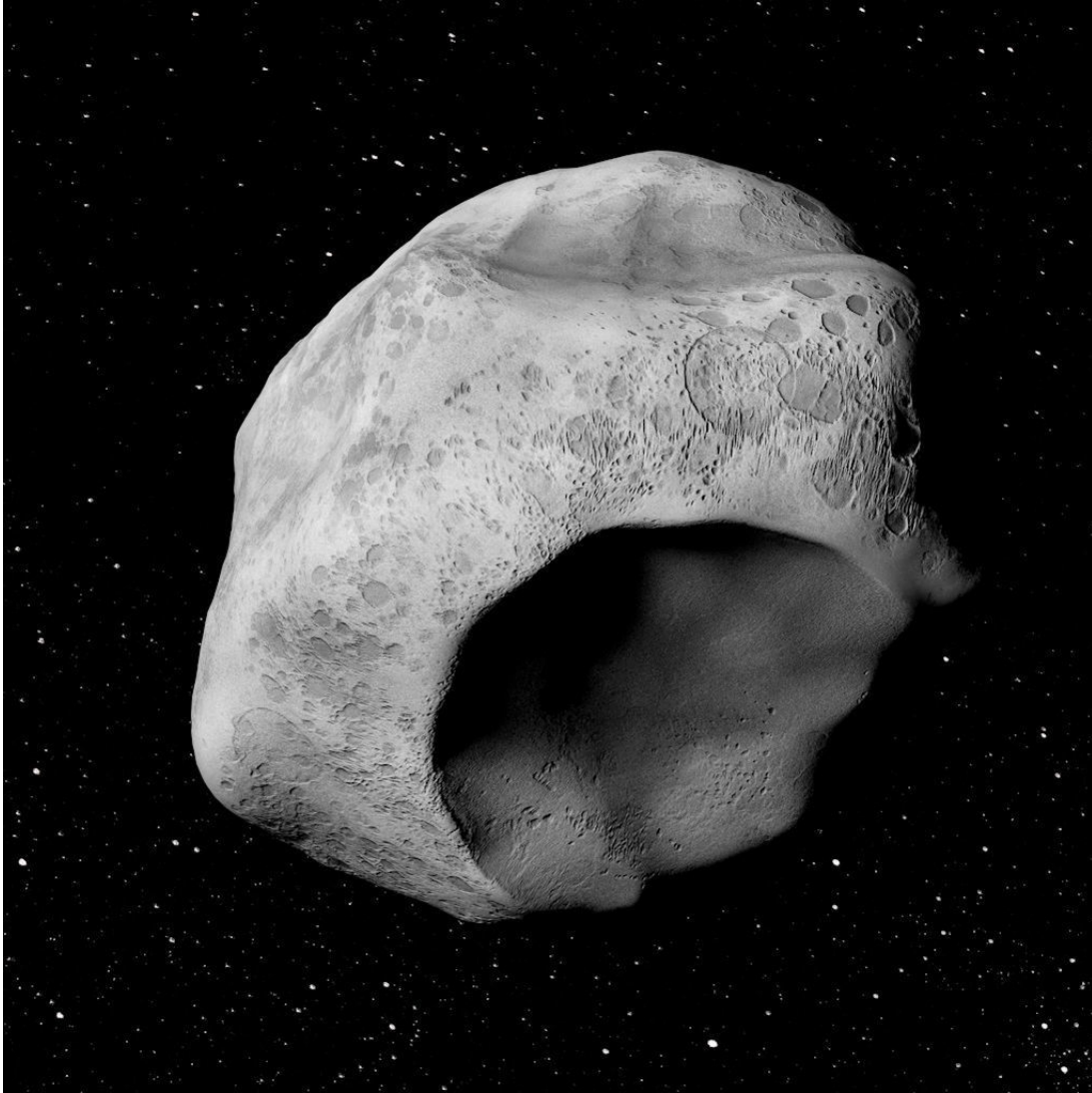


Figure 1.1: 3D model of 253 Mathilde based on the pictures from NEAR's fly-by

to take detailed pictures of the surface of Mathilde, which is still largely unknown. Pictures of other planets/asteroids encountered during the heliocentric transfers to the final target should also be taken.

The data from the on-board IMU will be recorded at the moment of touching the asteroid's surface for the sample retrieval: the dynamic recording of landing/bouncing events should give insights into the soil's mechanical properties.

CHAPTER 2

Environment

The orbit of the target asteroid 253 Mathilde is represented by the parameters in Table 2.1

a [AU]	2.648
e	0.2649
i [deg]	6.74
Ω [deg]	179.6
ω [deg]	157.4

Table 2.1: 253 Mathilde orbital parameters

Because of the orbit's high eccentricity there is a great variation of the solar irradiance during one period: Mathilde receives 364.90 W/m² at the perihelion (1.95 AU) and 123.11 W/m² at the aphelion (3.35 AU).

There is no direct evidence regarding the presence (or absence) of dust around Mathilde. According to [Lee \(1996\)](#) electrically resistive planetary surfaces can evolve charge differentials when exposed to solar radiation, leading to particle levitation (see Appendix, Figure 1). Due to its composition and long rotation period (417.7 h), Mathilde could present levitation (and even escape) of particles 50 μm in radius.

The NEAR probe found no surface magnetic field on the asteroid Eros and according to [Wilkinson \(2009\)](#) it is unlikely that any asteroid would have a strong or even measurable magnetic field (except for M-Type which are still under examination). This, combined with the long heliocentric legs necessary to reach Mathilde, means that the s/c will be subjected to high levels of radiation. To give an order of magnitude, the estimated radiation dose associated to a 3 year mission to Mars is 1800 mSv ([Vercoutere et al. \(2008\)](#)). For this reason on-board electronics and payloads shall be either shielded or inherently resistant to similar or higher levels of radiation, as the mission is expected to last upwards of 5 years. Mission-critical components shall be tested for SEE.

Dimensions [km]	66×48×46
Surface gravity [km/s ²]	0.00989
Rotation period [h]	417.7
Albedo	0.0436
Surface temperature [K]	174 - 245

Table 2.2: 253 Mathilde physical characteristics

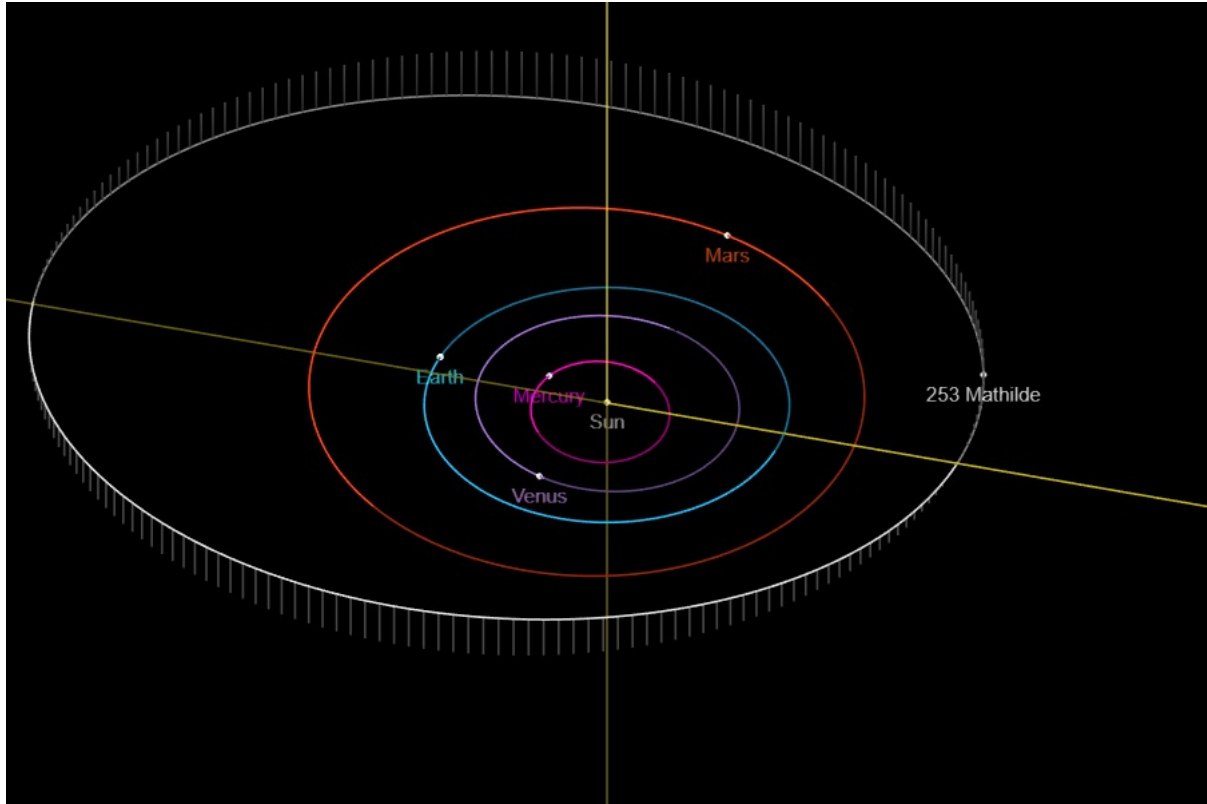


Figure 2.1: Orbit of 253 Mathilde

With a surface gravity of 0.00989 m/s^2 Mathilde's gravitational field is very weak. This means that the main orbital perturbations will be due to SRP and the influence of Jupiter and the Sun rather than irregularities in the asteroid's mass distribution. The effects of those perturbations are non-negligible considering the duration of the mission. Because of the weak gravitational field and the absence of atmosphere the s/c will constantly operate in micro-gravity and vacuum, so the s/c components and payload shall be chosen, tested and built accordingly. In particular, the bacteria shall be able to survive and proliferate in those conditions.

CHAPTER 3

Mission architecture

3.1 Preliminary architecture selected

There is a big amount of configurations and architectures that can be adopted in order to achieve the goals of the mission.

A preliminary distinction can be done between a completely autonomous one and, on the other hand, the possibility to share part of the trajectory with an already planned mission. For MIDAS, since the only potentially advantageous "mothership" could have been Psyche, targeting *16 Psyche*, which is expected to be launched in 2022, the autonomous option has been selected. In fact, a too early departure would have required an actual TRL of 8/9 for every component of the spacecraft, which is not the case since many of them need a further development in next years. Moreover, a mission such as Psyche would have put a very big constraint regarding the trajectory selection, the target and the satellite configuration as well.

A secondary difference is in what concerns the trajectory adopted in order to reach 253 Mathilde. As can be seen in Figure 3.1 and in Figure 3.2, the direct transfer requires a very elevated cost in terms of Δv both for launch phase and for arrival phase.

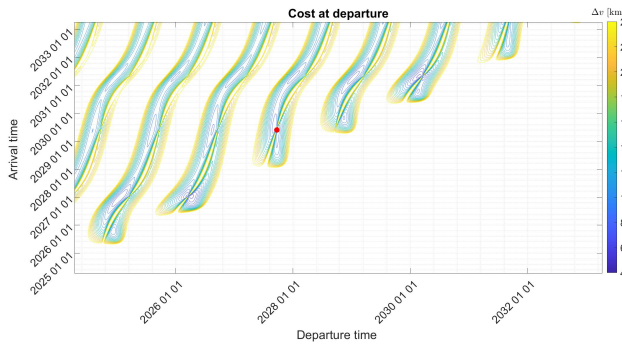


Figure 3.1: Direct transfer Launch cost

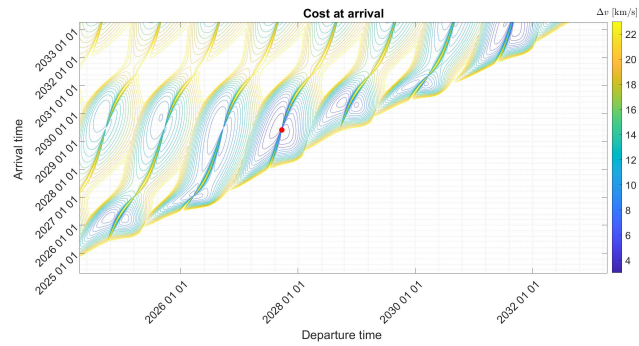


Figure 3.2: Direct transfer Arrival cost

A Gravity Assist option has to be considered, as can be seen in section 3.2.

Last but not least, there are two main possibilities concerning where the experiment will take place: directly on the asteroid after landing or, alternatively, on orbit after a sample collection with a *Touch And Go* manoeuvre. The second one has been selected, due to the fact that it is easier to develop, it is more flexible and can be repeated in case of failure, it is more controllable and puts less constraints and requirements on what concerns the spacecraft structure, electrical, thermal and propulsion subsystems and the payload needed.

3.2 Trajectory

As previously said, MIDAS mission does not involve any mothership, thus a trajectory has been selected in order to size the launcher and Δv requirements. Computations have been done starting in 01/01/2035 and arriving in 01/01/2048 (reasonable dates since TRL upgrade is needed for at least 2 years per step from TRL 3 on, for the majority of the components that shall be on board). Data for Mathilde orbit have been computed using JPL Horizon ephemeris while all computations have been performed using MATLAB.

The Patched Conics Method has been used, linking two Lambert Arcs with a Gravity Assist around Mars. It is important to underline that this is an approximate method; in particular, the most important simplification adopted is that every manoeuvre involved is expected to be an impulsive one, so this will influence the selection and the sizing of the propulsion system. Furthermore, the results obtained comes from an optimization process (using a Genetic Algorithm and Random Search Algorithm implemented in MATLAB), but it can be improved in order to obtain better results.

In Figure 3.3 and in Table 3.1 the results of this analysis are shown.

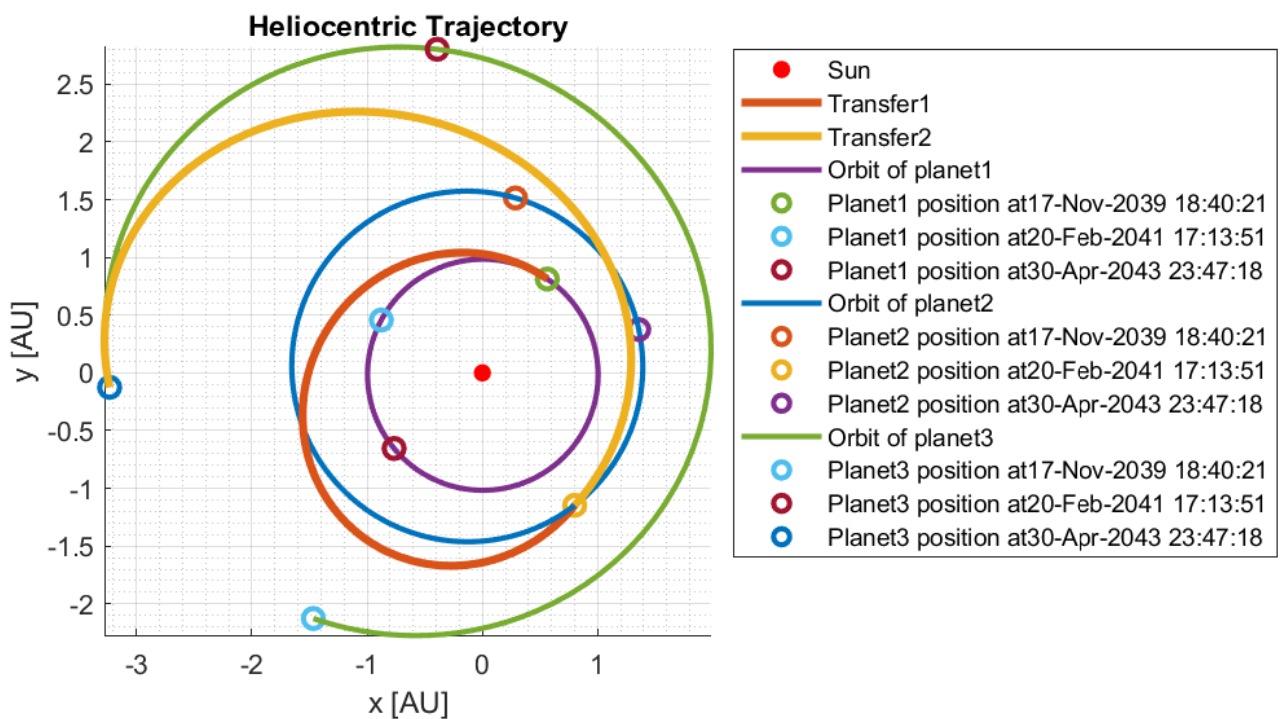


Figure 3.3: Heliocentric Trajectory with Mars GA strategy

This trajectory is advantageous as it is a compromise between short time and weak impulses, but it requires engines that can provide both high specific impulse and high thrust in order to achieve a quasi-impulsive manoeuvre with a very low amount of fuel consumption (storage is limited by constraint on volume (Max 24U) and configuration).

Parameter	Results
Δv_{launch}	3.97 km/s
Δv_{ga}	0.009 km/s
Δv_{arr}	2.79 km/s
Δv_{tot}	6.73 km/s
Total Time	1260 days

Table 3.1: Transfer characteristics

3.3 Conceptual operations

In Figure 3.4 an overview of the mission timeline with its main phases can be seen. In particular the two legs of the trajectory takes more than 1 year and more than 2 years respectively. As shown in subsection 3.3.4, a standby mode is required and it is expected to last 1 year, as well as the experimental part of the mission.

Each phase will be thoroughly analyzed starting from Launch.



Figure 3.4: Mission Timeline

3.3.1 Launch

A first estimation of the Δv_{launch} is 3.97 km/s. Hence the launcher has been selected based on the expected mass (~ 28 kg) and the C3 required (15.76 km/s). According to Figure 3.5 all medium launchers can provide this value of C3 to the spacecraft, in order to put it directly onto the first Lambert leg of the trajectory. There aren't programmed missions in the main asteroid belt in those years hence the launch is not expected to be shared at the moment. With the aim of reducing costs, the launcher should be shared with at least another mission with a similar objective.

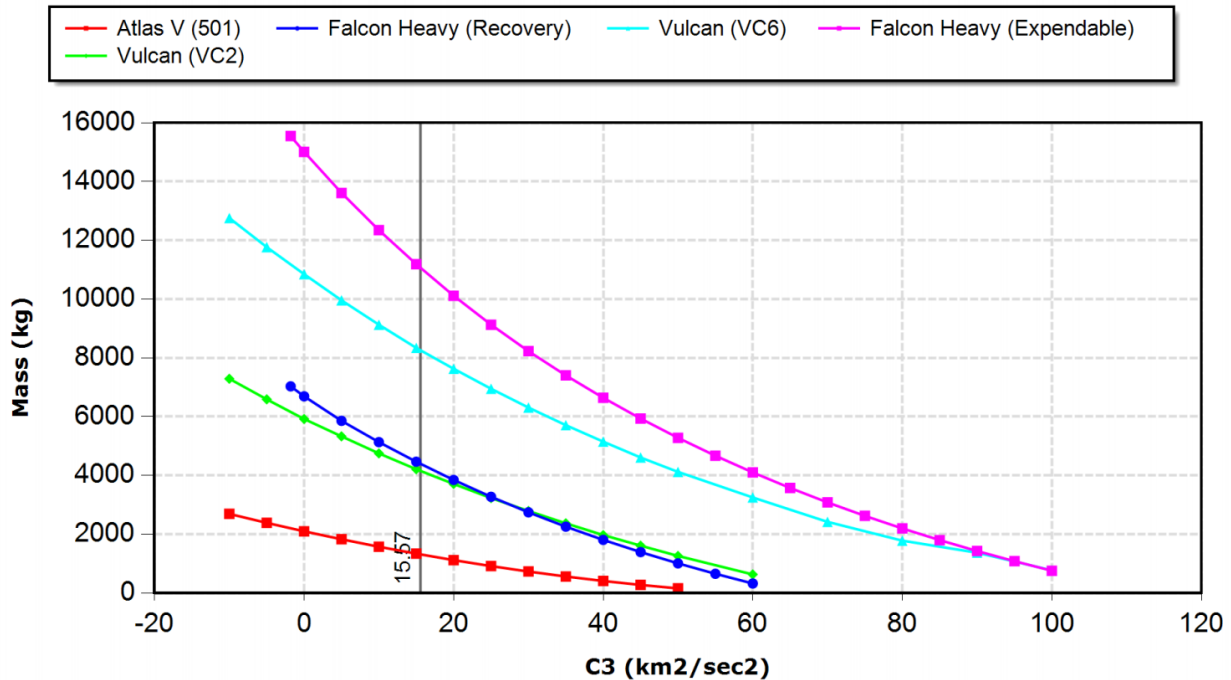


Figure 3.5: Launchers C3 vs Mass

3.3.2 Detumbling and cruise mode

After launch phase, a beacon communication needs to be established using an isotropic antenna with the on ground segment. Then detumbling phase will start to set the attitude required during travel and solar arrays will be deployed and pointed to the sun using actuators moved by a pre-charged secondary battery.

During the travel both on first and on second leg of the trajectory, two main things shall be taken into account:

- The position of the spacecraft shall be communicated regularly to avoid or at least minimize position and target errors;
- The health of both the spacecraft itself and the payload shall be assured during the whole life of the mission, in order to maintain everything alive, in particular temperatures must be kept inside the *vital range*.

3.3.3 Mars Gravity Assist

At the moment of the Gravity Assist around Mars, a communication of the successful manoeuvre is needed. For this aim, an high gain antenna has been selected, as the distance between Mars and Earth at the moment of the GA could be up to 3 AU (this is the case, as can be seen in Figure 3.3). Secondary battery, recharged during the first leg using solar arrays, shall be sufficient for the telecommunication mode, so this phase relies mostly on battery power supply.

The GA manoeuvre which provides the minimum Δv has the following characteristics:

- Total ΔV provided by the GA: 5.02 km/s (of which 9 m/s shall be given by the engine)
- Impact parameter: 5256 km
- GA altitude: 871 km
- Time spent inside Mars Sphere of Influence: 47 hours

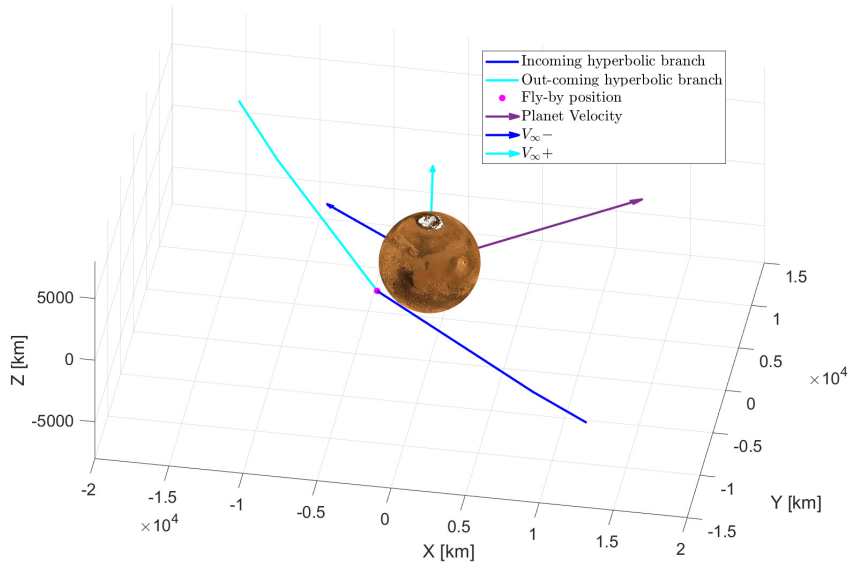


Figure 3.6: GA Heliocentric Hyperbolas

According to the GA characteristics shown before it is possible to take scientific images of Mars during the manoeuvre.

Two big issues must be taken into account at and before the GA phase. First of all the spacecraft shall be able to point correctly Mars and, in particular, a region where the GA can be considered both safe and successful. Secondly, Planetary Protection normative must be considered: according to the International Planetary Protection Handbook, Mars gravity assist is part of Category III. It means that one of the two following possibilities shall be satisfied:

- The probability of impact on Mars by any part of a spacecraft assembled and maintained in ISO level 8 cleanrooms, or better, is $\leq 10^{-2}$ for the first 20 years after launch, and $\leq 5 \cdot 10^{-2}$ for the time period from 20 to 50 years after launch (e.g., Mars Express, TGO).
- The total bioburden of the spacecraft, including surface, mated, and encapsulated bioburden, is $\leq 5 \cdot 10^5$ bacterial spores (e.g., MRO, Maven).

The second one is unfeasible since the experiment involves more than $5 \cdot 10^5$ spores hence the first one is required.

In order to avoid any possible contamination of the planet, two things were considered:

- Bacteria killing mechanism, made of heaters directly applied onto the bacteria culture to rise up temperature over their vital range
- Constraint on the GA altitude. The Gravity Assist shall take place at an altitude of at least 100 km. This value was put inside the trajectory optimization algorithm, excluding the unsafe solutions. A chart confirming that this manoeuvre can be considered a safe one is shown in Figure 3.7, where can be seen that at 100 km altitude the density of Mars atmosphere is almost negligible.

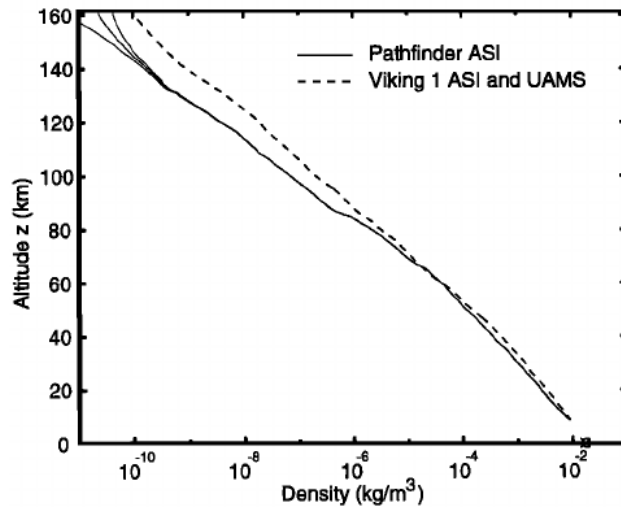


Figure 3.7: Mars atmosphere density estimated by Viking mission

An overview of the total cost for the GA and navigation phases, that shall be entirely provided by the propulsion subsystem, can be seen in Table 3.2

Parameter	Value
$\Delta v_{poweredGA}$	9 m/s
Δv_{GA}^*	15 m/s
Δv_{nav}^*	10 m/s
Δv_{total}	34 m/s

Table 3.2: Cost required by the engine during navigation and GA.

* Safety margin coming from a preliminary sizing both for GA and navigation phases

3.3.4 Arrival and stand-by mode

At the arrival phase a very intense burn is required, as can be seen in Table 3.1, in order to be capture by the asteroid gravity field and rendezvous with 253 Mathilde.

The sphere of influence of Mathilde can be calculated using this formula:

$$r_{SOI} = r_{MS} \cdot \left(\frac{m_M}{m_S} \right)^{\frac{2}{5}} \quad (3.1)$$

where:

- $r_{MS} = 3 \cdot 1.496 \cdot 10^8 \text{ km}$, is the distance between Mathilde and the Sun at arrival
- $m_M = 1.033 \cdot 10^{17} \text{ kg}$, is the Asteroid mass
- $m_S = 1.98855 \cdot 10^{30} \text{ kg}$, is the mass of the Sun;

obtaining the following result at approximately 3 AU, since the rendezvous is expected to happen near Mathilde aphelion: $\mathbf{r}_{SOI} = \mathbf{2179.106 \text{ km}}$.

According to this result, the capture burn will happen at, approximately, a safe altitude of 200 km above Mathilde. This distance is the apogee of an high elliptical capture orbit with a perigee of 25 km, expected to be safe and near enough for imaging. At the perigee of this orbit another very small burn (12.9 m/s, impulsive approximation) will be performed in order to circularize the trajectory around the asteroid and enter the final orbit. Then, the so called "standby mode" will be activated as the solar arrays can't supply the required power to the main payload until the distance from the sun will drop under 2.5 AU. During the standby mode, several images of 253 Mathilde will be taken from different angles and stored in memory in order to have a wide data characterization of the planet before the main mission starts. This architecture allows the best compromise between mission time and solar array area. At this mode the solar panels shall be able to recharge the secondary battery only, needed for communications.

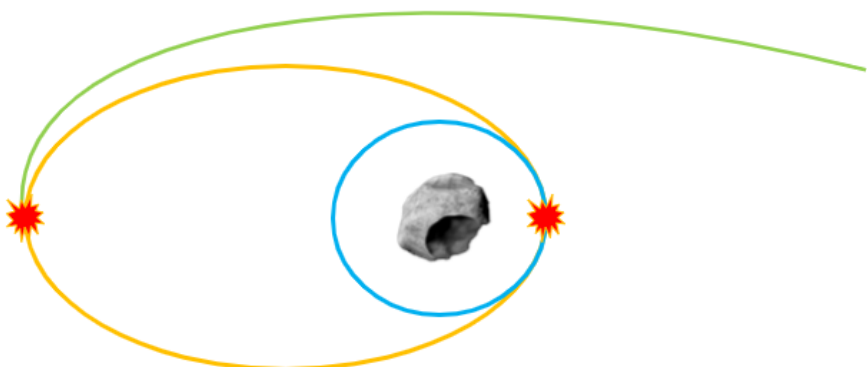


Figure 3.8: Capture orbit

3.3.5 Observation on Orbit and Touch and Go procedure

After the standby mode, at the proper distance less than 2.5 AU all the main operations can be started. The observation campaign for the best possible touch and go spot identification will be carried on and finished as soon as possible. It is expected to last some weeks, after which the descending phase to the identified spot will begin. Here, a tail-down attitude configuration is needed, as well as LIDAR measurements and accurate vertical faring using the engine, that is required to give approximately 19 m/s impulse in this phase in order to reach a zero relative velocity with respect to the asteroid. This last value has been computed according to [Owen E. Maynard \(1966\)](#), calculated as 1.18 times the velocity that the spacecraft would have along an orbit with zero altitude around Mathilde, as if it were a sphere. To support this choice, the additional margin suggested by ESA is +20% of the landing manoeuvre.

Before the descent, the Touch And Go Sample Acquisition Mechanism (TAGSAM) must be deployed. The sample will be collected staying approximately for 5 sec in contact with the surface. After sample retrieval, a re-ascending phase is planned, requiring approximately the same amount of impulse needed for the previous phase. The spacecraft will return back to the safe and circular parking orbit at 25 km altitude in order to perform the experiment.

Before that, a mass evaluation is required as a method to characterize the whole previous manoeuvre both if it was a successful one and if another Touch and Go procedure shall be repeated. To determine the mass of collected sample, the spacecraft implements a delta moment of inertia technique. Prior to sample collection, while in orbit, the spacecraft conducts a series of slow spins with the arm extended. There are two spins, both about the z-axis ([May et al. \(2014\)](#)). The first extends the arm along the z axis, the second extends the arm along the x axis (Figure 3.9). These provide a baseline measurement of the spacecraft angular momentum without any sample. This procedure is then repeated with the sample collected. The change in moment of inertia is a direct measurement of the sample mass. In order to achieve this measurement the sensors and actuators shall be accurate enough to detect the slight change of moment of inertia caused by the sample mass, which is expected in the order of grams. If this requirement proves to be too stringent to be satisfied, an alternative mass evaluation technique shall be designed and implemented.

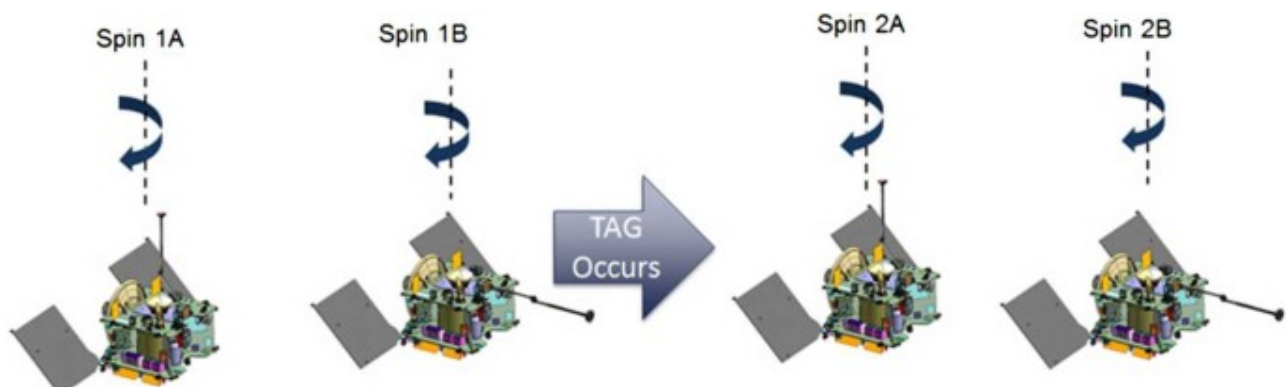


Figure 3.9: Delta moment of inertia technique, OSIRIS-REx

All in all, an overview of the total cost for the arrival and Touch and go phase, that shall be entirely provided by the propulsion subsystem, can be seen in Table 3.3

Parameter	Value
Δv_{arr}	2790 m/s
$\Delta v_{circularization}$	12.9 m/s
$\Delta v_{descending}$	19 m/s
$\Delta v_{ascending}$	19 m/s
Δv_{total}	2865.9 m/s

Table 3.3: Cost at arrival with a first-successful Touch and Go.

3.3.6 Experiment and Telecommunication

Once on orbit around the asteroid and after a positive mass evaluation, the sample collected shall be stored within bacteria colony in order to start the experiment and the methane generation. An amount of few ppm of gas is both expected and required to be produced by the culture in order to be detected and so to classify the whole mission as a successful one. For the experiment itself, a duration of 1 year shall be taken into account for two main reasons:

- Bacteria could take that time until they can generate biogas from the sample
- The idea is to exploit the nearest part of Mathilde orbit to the Sun, so 1 year is, approximately, the duration of the asteroid motion at the turn of its perihelion.

During this phase, the main telecommunication mode is planned to be on, in order to transmit the major part of data and images collected during the mission; for this aim, during that period, the most part of payload and sensors shall be off in order to guarantee the necessary power demand.

In Figure 3.10 all the subsystems and payloads expected to be in mode ON/OFF during each main phase are shown. Highlighted in yellow, in particular, all the subsystems that shall always be ON in order to maintain the spacecraft alive.

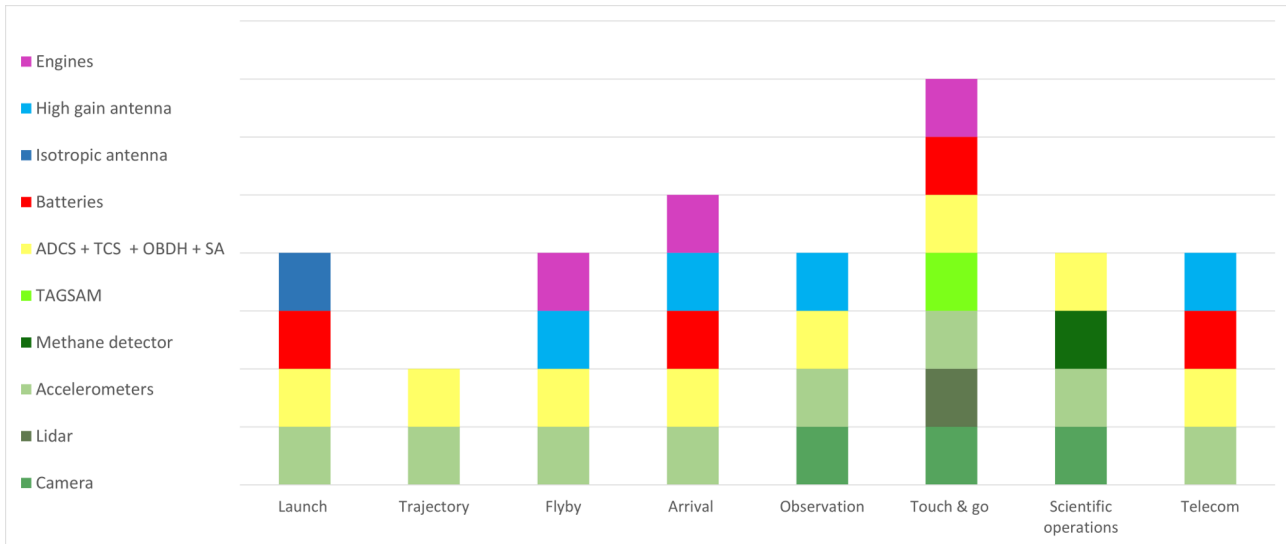


Figure 3.10: Active systems and payloads for every mission phase

3.3.7 End of Life

For disposal phase of the mission it has been decided to perform a soft landing on the asteroid. This is possible only before the bacteria killing mechanism has been switched on, otherwise Planetary Protection rules would not be respected. The Δv_{EOL} expected for the soft landing will be ~ 10 m/s.

CHAPTER 4

Sensors and Payloads

4.1 Bacteria selection

The appropriate bacteria to satisfy the mission requirements shall be methanogens bacteria able to survive in micro-gravity environment with mid-low temperature and high levels of radiations. According to [Klas et al. \(2015\)](#) and [Cavicchioli \(2002\)](#) psychrophilic bacteria can proliferate at temperatures $<-15^{\circ}\text{C}$ with a minimum of -18°C with no air needed (anaerobic bacteria). In addition the bacteria can be cold-adapted to survive till -28°C . However it has been noticed a significant reduction of metabolic activities below -40°C . Deinococcus radiodurans bacteria are also called polyextremophiles for their capability to survive up to 20 kGy of gamma radiation and a pressure as low as 10^{-5} Pa which makes them the optimal methanogens specie to survive in the deep space.

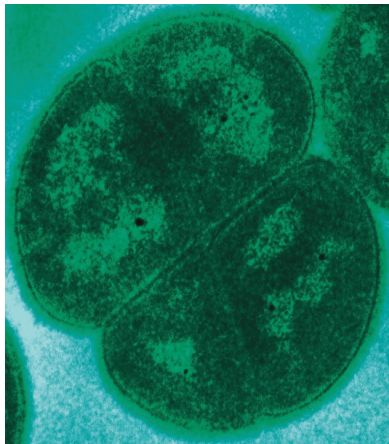


Figure 4.1: Deinococcus radiodurans

Parameter	Characteristics
Metabolic range	$-28^{\circ}\text{C} < T < 15^{\circ}\text{C}$
Survival range	$-40^{\circ}\text{C} < T < 60^{\circ}\text{C}$
P_{min}	10^{-5} Pa
Radiation	up to 20 kGy

Table 4.1: D. radiodurans characteristics

4.2 Bioreactor & Methane detector

The main payload which has been used to acquire methane data is the methane detector. This latter device should be directly coupled with the bioreactor where the methane production takes place. Measurements shall be taken at least 1 per second.

Parameter of coupled system	Requirement
Volume	< 1 U
Mass	< 1 kg
Power	< 100 mW
Accuracy	< 1 ppm
Radiation resistance	Deep space

Table 4.2: Bioreactor & Methane sensor system requirements

4.2.1 Bioreactor

Bioreactor is a device capable of performing automatic cell culture of bacteria, for this case in a micro-gravity environment. It is equipped with reservoirs for chemicals (which will be filled with the chondrite material) and a culture chamber allowing cell growth as shown in Figure 4.2.

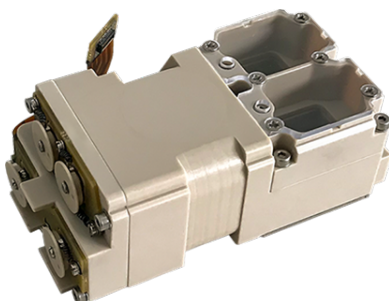


Figure 4.2: Bioreactor, Kayser Italia

Parameter	Characteristics
TRL	9
Dimensions	82 × 39 × 29 mm
Mass	146 g

Table 4.3: Bioreactor requirements and constraints

This payload is TRL 9 since it has been used for years in the ISS experiments hence it also has a good reliability.

4.2.2 Methane detector

The methane detector has been calibrated according to the expected methane production rate ([Mauerhofer et al. \(2021\)](#)) which on Earth environment is approximately 0.1 mmol/L h. In micro-gravity conditions ([Cockell et al. \(2020\)](#)) with non-biological control the production rate is also suppose to be bigger than the one on Earth. According to [Aldhafeeri et al. \(2020\)](#) nowadays methane detectors have different working mechanism thus it has been selected the one that suits best the mission which means most accuracy measurements: 0.7/2.9 ppm .

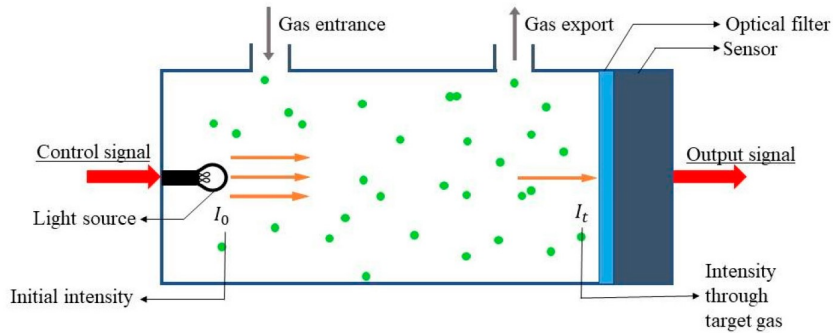


Figure 4.3: Optical gas sensor

Optical gas sensors detect changes in visible light or in electromagnetic waves that result from an interaction of the analyte with the receptor part. Methane gas is a gas characterized by a strong absorption at a wavelength between 2.3 and $3.26\mu m$ hence can be detected by a diode laser optical sensor. In Triki et al. (2015) it has been proposed two kind of sensors which works in this way:

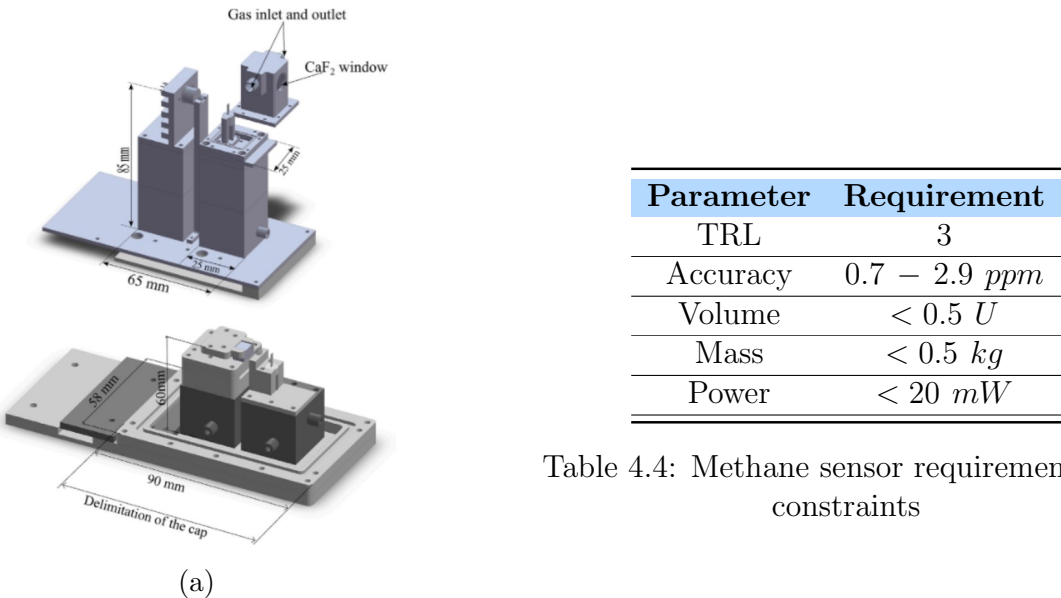


Table 4.4: Methane sensor requirements and constraints

Figure 4.4: Methane optical sensors variations proposed

4.3 VIS-NIR Camera

In order to achieve both primary, ancillary objective and for proximity relative navigation, a ultra-compact imager is needed. A very detailed set of observations are planned during the arrival phase of the mission and along its orbit around Mathilde before starting the landing sequence, with the purpose of identifying the best landing spot both in terms of safe (avoid craters, shadow zones, uneven terrain and dense dust regions) and soil composition (search

for high carbon composition regions). High capacity and high performance mass storage are required in order to store, elaborate and send the images and the information collected. Good pointing is required in order to get the best possible images. The VIS-NIR camera used in ASPECT mission ([Kohout et al. \(2017\)](#)) suites exactly the following requirements and should be set with the near infrared frequency in a range between $0.7\text{-}4.0 \mu\text{m}$ wavelength ([Larson et al. \(1979\)](#)) according to which specific kind of C-Type Mathilde is, still requiring a more detailed study.

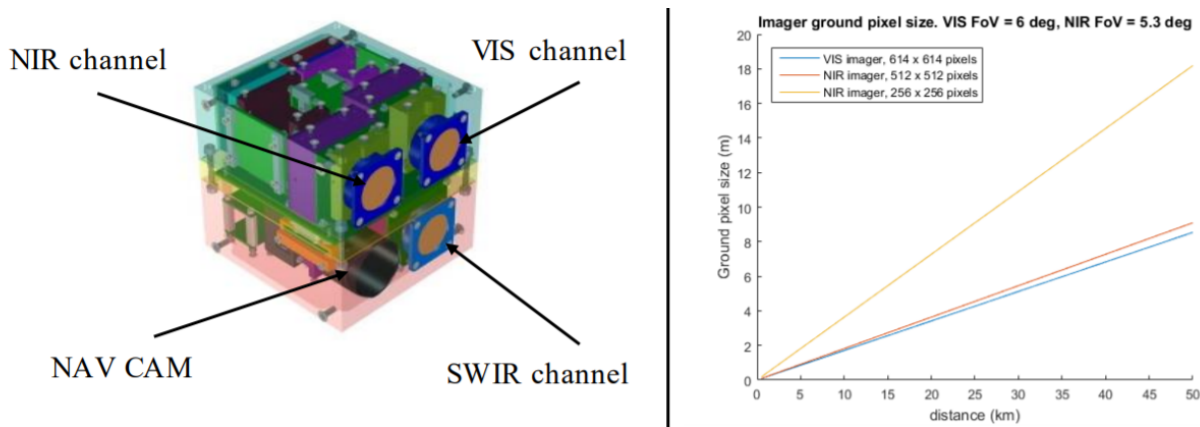


Figure 4.5: VIS-NIR ASPECT camera

Parameter	Requirement
Mass	$< 1 \text{ kg}$
Dimensions	$\leq 1 \text{ U}$
Power usage	$< 5 \text{ W}$
Operating range	$-10^\circ\text{C} < T < 40^\circ\text{C}$
Radiation tolerance	$> 5 \text{ years in deep space}$
Resolution	$< 1 \text{ m at } 25 \text{ km altitude}$
Spectrum	<i>VIS for observations – $0.7\text{-}4.0 \mu\text{m}$ wavelength for soil composition</i>

Table 4.5: Camera requirements and constraints

4.4 LIDAR

Vertical distance measurement is particularly important to ensure low risks during one of the most critical phases of the mission. Even though the landing site will be accurately chosen, the vertical velocity must be kept below a certain limit (defined by the TAGSAM requirements) in order to guarantee a correct sampling process; this is particularly true considering the difficulty to provide very accurate ΔV manoeuvres due to the asteroid low gravity field. Therefore, to provide enough precision, while keeping the mass and accuracy as a figure of merit, a LIDAR similar to the Jenoptik DLEM-20 may be chosen, with its 33 grams and very good accuracy up to 1500/2000 meters. The maximum measurable distance should reach up to 4/5 km for increased safety. The LIDAR can be used also for relative position with respect to Mathilde for

state vector determination and, if possible, local ground morphology analysis (together with camera, as a scientific payload).



Figure 4.6: Jenoptik DLEM 20

Parameter	Requirement
Mass	$\leq 0.04 \text{ kg}$
Volume	$\leq 0.05 \text{ U}$
Power usage	$\leq 1.5 \text{ W}$
Operating Temperature	$-20^\circ\text{C} < T < 60^\circ\text{C}$
Survival Temperature	$-25^\circ\text{C} < T < 80^\circ\text{C}$

Table 4.6: LIDAR requirements and constraints

4.5 Accelerometer and gyroscope

The main functionality of the accelerometer is to provide state vector determination by sequence integrations or, if star tracker are present, could still provide a desirable redundancy in the ADCS. Obviously, to avoid greater and greater errors, constant realignment is needed (for example through ground communications or, again, star sensors). As a scientific payload, during the touch and go phase it can also be exploited to perform a dynamic recording of landing/bouncing event, in a similar way to what Juventas mission (Goldberg et al. (2019)) is going to do. Since this sensor shall be operative for the whole mission, the driving requirements are power usage and resolution. Especially the latter is of significant concern since the asteroid gravity field is very low. A reasonable value have been set to $1 \mu\text{g}$, approximately a thousand

times less than Mathilde (this value has been set the same as Juventas mission, which is analysing a much smaller body). Therefore, a good candidate is represented by the Senonor Stim-300, with its 55 grams, 2 W of power demand and right on spot resolution; it's a complete IMU, with 3 accelerometers and 3 gyroscopes, which can be exploited to improve the ADCS accuracy and to provide the attitude estimation during the short eclipse time.



Figure 4.7: STIM-300 accelerometer

Parameter	Requirement
Mass	$\leq 0.06 \text{ kg}$
Volume	$\leq 0.05 \text{ U}$
Power usage	$\leq 2 \text{ W}$
Accelerometer Resolution	$\sim 1 \mu\text{g}$
Operating Temperature	$-40^\circ\text{C} < T < 85^\circ\text{C}$

Table 4.7: LIDAR requirements and constraints

4.6 TAGSAM

Touch And Go Sample Acquisition Mechanism (TAGSAM) is the same payload used in Osiris-Rex mission in order to collect the chondrite present in the soil. This payload, as shown in Figure 4.8, blows the inert pressurized flow kept inside the tanks (N_2) and filters the bigger particles with a screen [Bierhaus et al. \(2018\)](#). All the material will be stored in the collection reservoir and then inserted inside the bioreactor. As for the Osiris-Rex, it has been required to stay 5 sec in touch with ground with a sample collection at least of $\sim 1\text{g}$. The landing target has been chosen according to the provided data by section 4.3 and then analyzed by scientists.

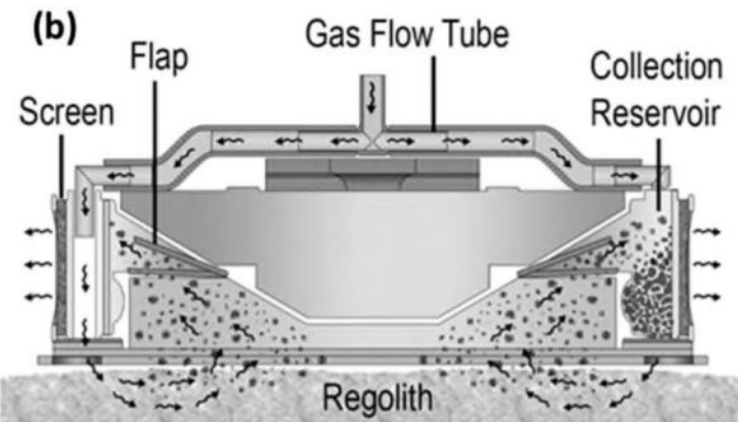


Figure 4.8: TAGSAM working principle

Parameter	Requirement
Temperature range	$-28^{\circ}C < T < 80^{\circ}C$
Pressure	Vacuum
Radiation	<i>Not to have structural problem during TAG</i>

Table 4.8: TAGSAM requirements

CHAPTER 5

Subsystems

5.1 Propulsion Subsystem

The propulsion subsystem shall provide a ΔV of nearly 3 km/s, in order to circularize the trajectory at Mathilde arrival. However cubesat primary propulsion still misses for interplanetary travels. Nowadays motors for small s/c imply unfeasible trade-offs, e.g. using a monopropellant engine, like the Busek BGT-X5, would lead to a total mass greater than 40/50 kg ($I_{sp} = 225$ s); at the same time, an ion engine (as the Busek Bit-3) has too low thrust for the manoeuvre to be impulsive (and thus too long energy-intensive operations). The best solution is given by high efficiency bipropellants, and in particular hydrogen and oxygen. To overcome the tank size problem, the two elements are stored as simple water, which is then convoyed to an electrolyzer when needed. Tethers Unlimited Hydros-C, currently in TRL 8, exploits this technology, reaching a specific impulse of 310 seconds, with a power consumption of less than 25 W and a *green* fuel.

According to Pothamsetti and Thangavelautham (2016) it's possible to further improve the performance by increasing the input power and the electrolyzer efficiency; moreover, it's possible to include specific additives to lower the freezing point below 0°C.

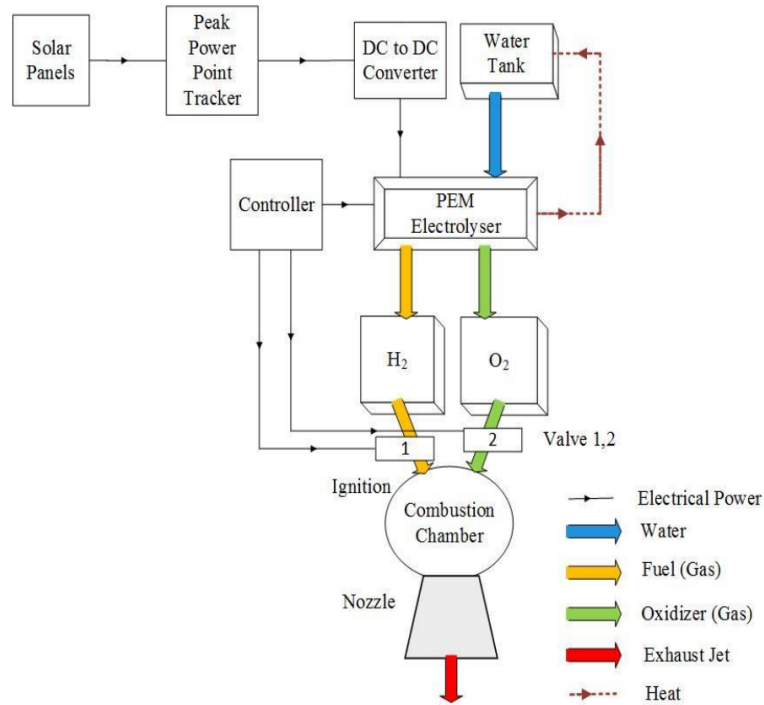


Figure 5.1: Photovoltaic Electrolysis Propulsion System for Interplanetary Cubesat

In the Table 5.1 below are listed the performance of the Hydros-C in comparison with the experimental improved version. Thanks to the PEM electrolyzer (efficiency up to 0.95) and an increased power usage of 60-90 W the specific impulse is now much greater, more and more similar to larger, pump-fed engines.

Engine	HYDROS-C	Experimental
TRL	8	3/4
Thrust[N]	> 1.2	Up to 8
I _{sp} [s]	> 310	Up to 424
Power[W]	5-25	60-90
Dry mass [kg]	1.4	1.9
Propellant type	Water	Water
Propellant mass [kg]	25	14
ΔV [m/s]	2910	2970
Burning time	5.6 h	3.1 h

Table 5.1: Hydros-C and Experimental characteristics

5.1.1 Mass breakdown

As a consequence of the analysis done above, the resulting mass breakdown is shown in Table 5.2 for the two different engines and their relative performance. Some values will be encountered later, during the description of the other subsystems. It's important to underline that these are, in general, optimistic and a more detailed analysis may be needed at a successive study phase. It is clear how much weight can be saved with an optimized propulsion system.

TOTAL MASS [kg]	40.6	27.5
Payload	2.50 ± 0.62	2.50 ± 0.62
Platform	0.089 ± 0.01	0.089 ± 0.01
ADCS	0.63 ± 0.13	0.63 ± 0.13
OBDH	0.3 ± 0.06	0.3 ± 0.06
EPS	1.6 ± 0.32	1.6 ± 0.32
TCS	0.1 ± 0.02	0.1 ± 0.02
TMTC	0.81 ± 0.16	0.81 ± 0.16
Engines	1.4 ± 0.28	1.9 ± 0.38
Propellant	25	14
Structure & Tanks	8.2 ± 1.64	5.5 ± 1.1

Table 5.2: Mass breakdown. ESA margin of 20% was considered, excluding propellant

5.2 Electrical Power Subsystem

5.2.1 Power breakdown

The EPS shall provide enough power to keep the spacecraft alive and perform scientific operations during the whole mission. In Figure 5.2 is shown the power breakdown for every mode identified.

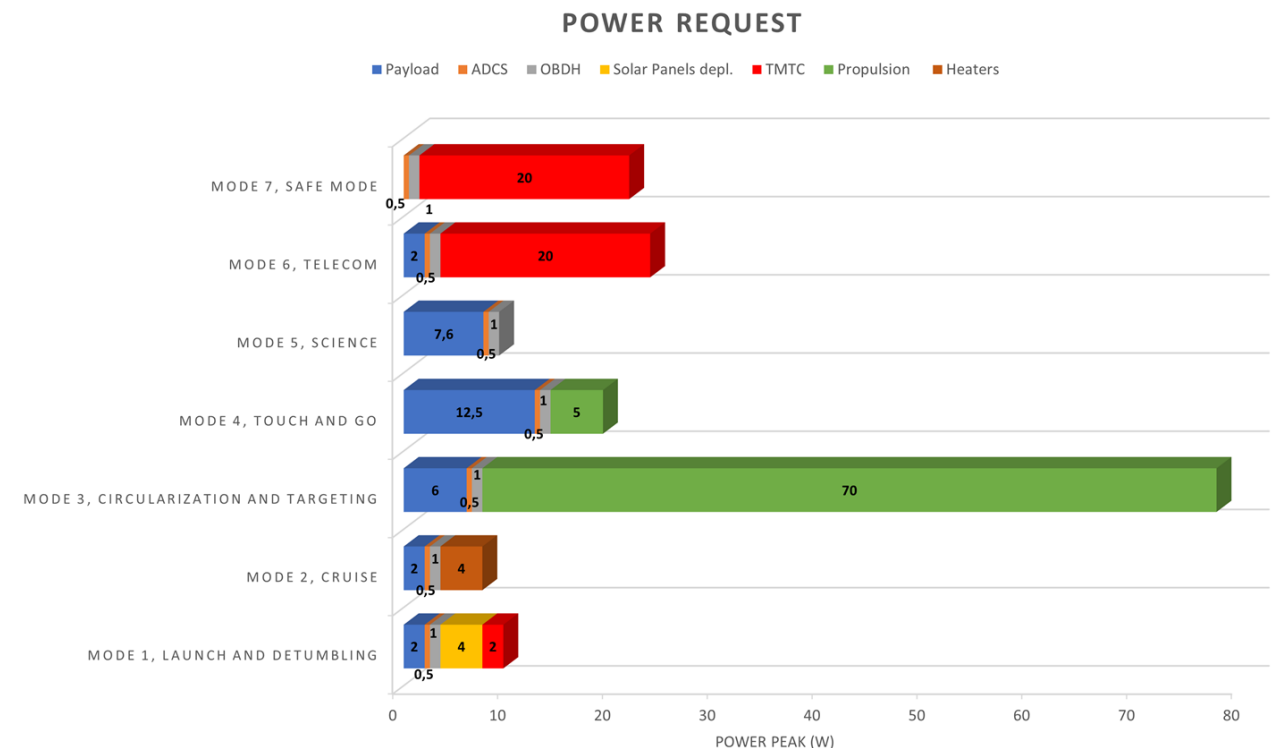


Figure 5.2: Power breakdown for the different modes

Due to the high energy-intensive Propulsion Subsystem, solar arrays and secondary batteries can't provide enough power, while keeping the weight as low as possible. On the other hand, the functioning time of the engine is limited to 3 hours, thus allowing to supply the necessary power using only a "one-shot" primary battery (thanks to its high energy density). Finally, considering the small size, the spacecraft EPS is based on a DET configuration (See Figure 5.3), with a slightly higher efficiency with respect to PPT, more common on larger spacecrafts.

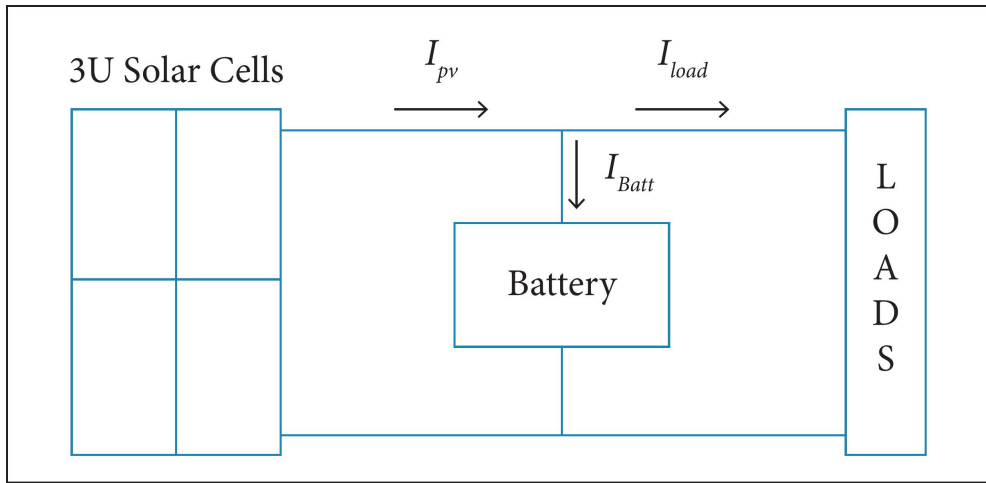


Figure 5.3: Scheme diagram of EPS in DET-3U topology

5.2.2 Solar Arrays

The design of the solar panels depends significantly on the irradiance coming from the sun and the overall efficiency and losses. Moreover, they shall recharge the secondary battery during daylight time. Considering a 14 hours period of a circular 25 km orbit around the asteroid, only two of them are expected to be in eclipse. It's important to notice that this is not necessarily a "shadow" time, but more in general the maximum amount of hours for which the battery is expected to operate. From the Figure 5.2 it's possible to see that the scientific operation phase has the highest long-term power consumption; therefore, the solar panels shall produce at least 10 W, considering approximately 10% margin. At the same time, the battery shall provide entirely the power for mode 6 and 7 (antenna operation, 25 W), as it can't be ensured that the solar panels will exactly point the sun during the telecommunication phase. Therefore, the required power to be provided in sunlight is approximately 18.2 W according to the following formula:

$$P_{sa} = \frac{\frac{P_e T_e}{X_e} + \frac{P_d T_d}{X_d}}{T_d} [W] \quad (5.1)$$

where:

- P_d : 10 W, minimum daylight power
- T_d : 12 h, time in sunlight
- X_d : 0.85, DET daylight coefficient
- P_e : 25 W, eclipse power
- T_e : 2 h, maximum eclipse time
- X_e : 0.65, DET eclipse coefficient

To compute the power per unit area converted by the panels, the following parameters have been considered:

- **Irradiance at 1 AU:** 1357 W/m²
- **Efficiency:** 0.29
- **Incident radiation offset:** 20°
- **Inherent degradation:** 0.75
- **EOL degradation (4/5 years):** 0.9
- **DET configuration**
- **Maximum distance:** 3.35 AU
- **Minimum distance:** 1.95 AU

Applying the equation:

$$P_{EOL} = \frac{P_0 \eta I_d \cos(\alpha)}{R^2} [W/m^2] \quad (5.2)$$

In this conditions, the power density converted by the panels varies between 23.7 W/m² (aphelion) and 69.8 W/m² (perihelion). It's clearly pointless to design them at the minimum distance from the sun, but also a significant overestimation at the aphelion. In fact, it is more convenient to set an intermediate distance (around 2.5 AU) for the scientific operation phase to start. In the meanwhile the s/c will perform the stand-by operations as described in Sec. 3.3.4.

5.2.3 Batteries

As already said above, due to the high power required by the engine, a **primary battery** has been adopted. Considering a Li-(CF)₂ non rechargeable battery, thanks to its energy density greater than 500 Wh/kg, the resulting weight is expected to be lower than 500 g, for a capacity required of 220 Wh. On the other hand, the **secondary battery**, a Lithium Ion one, is rechargeable, with an energy density of 220 Wh/kg and Depth Of Discharge of 0.8, sufficient for more than 2000 cycles (Elshurafa and Aldubyan (2019)). With these parameters the capacity is about 65.89 Wh, and the resulting weight is set to 300 g. Both batteries have been considered with an efficiency of 0.95. To guarantee the performance showed for the latter, approximately at half mission, reconditioning is needed: the battery will be completely discharged and recharged again (if solar arrays are available for the whole time).

Secondary battery capacity equation:

$$C_r = \frac{P_e T_e}{(DOD)\eta} [Wh] \quad (5.3)$$

5.3 Thermal Control Subsystem

The TCS is designed to keep the temperature of the systems within their design limits. The spacecraft has been considered as a 3 surface body, with each pointing at the Sun, Mathilde and deep space. This 3-node analysis allows to plot accurate results, while keeping the computations simple and thus readily verifiable (credits to Professor M.G.Guilizzoni). In Table 5.3 are shown the temperature ranges, both for the operating case and the standby (where the requirements are not as tight).

Payload	Operating range	Survival range
Bacteria	-28°C/+15°C	-40°C/+60°C
VIS-NIR	0°C/+30°C	-20°C/+70°C
Batteries	-50°C/+75°C	-50°C/+75°C
Methane det.	-30°C/+10°C	-40°C/+40°C
LIDAR	-20°C/+60°C	-20°C/+60°C
TAGSAM	-35°C/+70°C	-35°C/+70°C
Star tracker	-25°C/+70°C	-25°C/+70°C
Sun sensors	-25°C/+70°C	-25°C/+70°C
RW	-20°C/+50°C	-20°C/+50°C
Antenna	-55°C/+80°C	-55°C/+80°C
Tanks	+0°C/+60°C	+0°C/+60°C
CPU	-20°C/+65°C	-20°C/+65°C
Solar panels	-165°C/+130°C	-165°C/+130°C

Table 5.3: Parameters assigned and chosen for mission.

The spacecraft encounters different environmental conditions, with different irradiation coming from the Sun and different levels of dissipated power inside. The two most critical situations occur during the arrival phase and low-power operations at Mathilde orbit. With a conservative 0.75 efficiency of the engine (typical PEM electrolyzer efficiency is > 90%), the power dissipated during the circularization is approximately 25 W, over a period of 3.1 hours; this is the hot case. On the other hand, the cold case is during standby mode where the spacecraft generate less than 4 W of power for quite a long time (up to a year). The adoption of Multi-Layer Insulation (MLI) is obviously needed, even though it must be properly chosen. If the emissivity is too low, the temperature during engine operation may rise up to 80°C/90°C; however, if it is too high, water in tanks may freeze (and other systems not work properly). For these reasons, the best solution is found in the middle, with a value of emissivity equal to 0.025 for all the surfaces and about 4 W of active electrical heaters to be employed if temperatures reach freezing point. The result of the analysis is thus shown in Figure 5.4 for both cases.

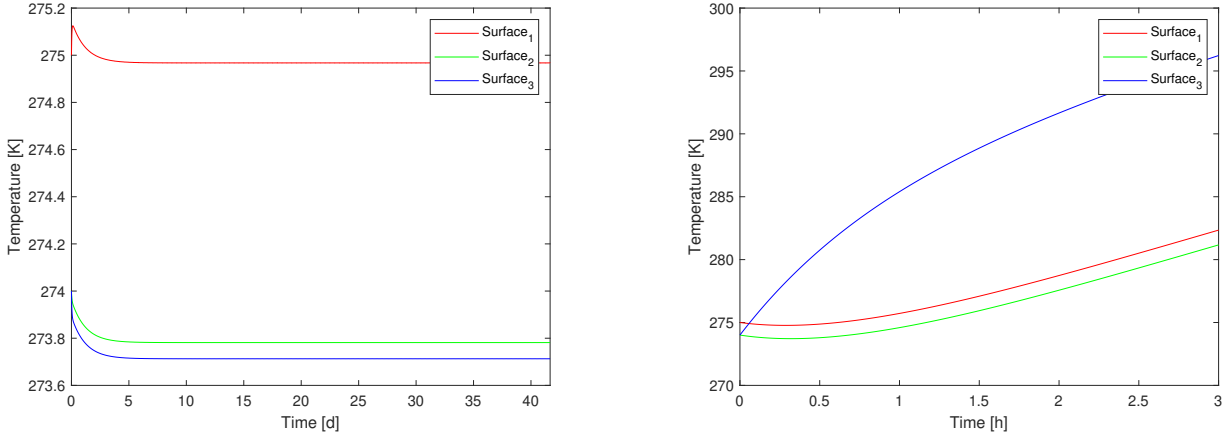


Figure 5.4: The cold (left) and hot (right) cases temperatures for the three surfaces

In the two most critical situations the temperature never exceeds 30°C and is always above 0°C. However, during propulsion phase it rises relatively fast on surface 3, thus meaning that if the engine needs to operate for more than 3 hours, a more detailed analysis should be done in order to prevent any hazard to the payload.

5.4 Telecommunication Subsystem

Data to be transmitted are divided in 2 phases:

- **detumbling phase:** beacon signal, telemetry, ADCS and state
- **deep space operations:** RGB images, NIR images, methane data, ADCS and state

According to their different requirements, it has been decided to select two kinds of antenna, one low gain and one high gain respectively for the two phases. The carrier frequency is in the Ka-band within a range based on ITU regulation that states (see Recommendation ITU-R SA.1014-3):

- uplink: 34.200–34.700 GHz
- downlink: 31.800–32.300 GHz

The polarization used is a circular one in order to avoid losses due to Faraday rotation and a linear receiver.

Downlink datarate is governed by the VIS-NIR images acquisition. The payload makes 614×614 pixels visible and 256×256 pixels infrared images. Thus each couple visible and infrared weights 9.6 Mb uncoded, while 19.2 Mb coded. The JPEG2000 (according to CCSDS 122.0-b-2) has been used to compress the images and its compression ratio is an adaptive one, however a good factor is 1:10 since images almost don't lose quality at all. The other scientific payload is the methane detector whose outputs are in the order of tens of bps coded. Telemetry data are

assumed in the order of 1 kbps coded. Therefore, the overall download rate is at least 10 kbps at the maximum distance.

BER selection:

- commands: 10^{-7}
- science: 10^{-5}

In order to increase the data rate an analog adaptive modulation has been chosen on three levels going from 16 QAM to 8 QAM and if needed from 8 QAM to 4 QAM when BER passes over the chosen threshold listed before. This allows to exchange symbols per second instead of bit per second, respectively 4,3,2 bit per second hence the data rate will be at least doubled and at maximum quadrupled.

The link must be achieved at a maximum of 3.5 AU which according to the orbit trajectory reported in section 3.2 it has been estimated to be the biggest distance.

The GS (Ground Segment) chosen is the DSN (NASA) (Figure 5.5) since the ESA GS hasn't an antenna with such requirements shown in Table 5.4.



Parameters	Antenna	Ground Segment
Gain [dB]	38	85
Power [W]	20	
T_{sys} [K]		21
d [m]	0.5	70

Table 5.4: Antenna transmitter and receiver characteristics

Figure 5.5: 70 m antenna, Canberra Deep Space Communication complex

Parameters	Link
Modulation index [%]	78
$L_{free-space}$ [dB]	-297
$L_{misalignment}$ [dB]	-0.5
L_{atm} [dB] *	> -2.5

Table 5.5: Link characteristics
* datum from Appendix, Figure 3

At the beginning of the mission (at 3.5 AU) the data rate will be at the minimum expected of 20 kbps for commands, while in the nearest point (at 2 AU) the maximum is in the order of 100 kbps for the payload.

5.4.1 Antenna

An antenna which shows very high performance is the reflectarray which has been already used in MarCo mission thanks to its wide aperture (high gain), good pointing, stowage, simplicity in deployment, reliability, low mass and cost. However according to Hodes et al. (2017) the gain is 28 dB which is not enough for our transmission system. For this reason it has been preferred a Ka-band mesh reflector (Chahat et al. (2016)), which has been already tested during the Rain Cube NASA mission.



Figure 5.6: Ka-band mesh reflector, JPL

Parameter	Requirement
Gain	42.5 dB
Data rate	20 kps
Dimension	1.5 U
Mass	< 0.8 kg
Power	22 W

Table 5.6: Antenna requirements

Data for the requirements have been taken according to Peral et al. (2018) and this technology is at TRL 7. Since the antenna is a critical element, all the possible failure modes shall be studied with FDIR and verification tests on them are required.

For the isotropic antenna (used during the detumbling phase) it has been chosen a solution of 4 low gain patch antennas placed on the external surfaces of the spacecraft, which provides low weight and bulk.

5.5 Attitude Determination and Control Subsystem

For the ADCS architecture it has been chosen the 3-axis stabilization configuration since there are stringent requirements on the pointing accuracy needed for HGA, 0.1° , and the camera, 0.01° . In addition the s/c shall also be capable of performing a touch and go. Sensors chosen for the state vector reconstruction are: sun sensors, star trackers, gyros. Attitude determination and estimation algorithms are required for programmed phases but also unexpected eclipse phase or unexpected failure of one or more sensors. Actuators chosen are:

- 4 reaction wheels disposed according to a pyramidal configuration, not to make them work at their maximum and having redundancy
- micro-propulsion thrusters which are cold gases that can be used both for fine pointing and desaturation of the reaction wheels

Perturbations expected are very low, almost negligible since SRP is very low due to the distance with respect to the Sun, magnetic field should not be present (and in the case it will be present,

the amplitude would be $\sim nT$), gravity gradient is not such a high perturbation when the s/c is small and when the mass around which it is orbiting is an asteroid.

Reaction wheels have been sized for a 2 min slew manoeuvre of 60° . The inertia of the spacecraft has been taken in the order of $100 \text{ kg} \cdot m^2$ (much more detailed analysis is required). At the end the torque required for each reaction wheel is $1.81 \text{ mN} \cdot m$. The same manoeuvre with micro-propulsion thrusters (or to desaturate the wheel after that manoeuvre) would require more time (~ 3 min).

Reaction wheels and thrusters with suitable performance can be found in retail catalogues for cubesats and are reported in Figure 5.7 and in Figure 5.8, though they require an important mass optimization.

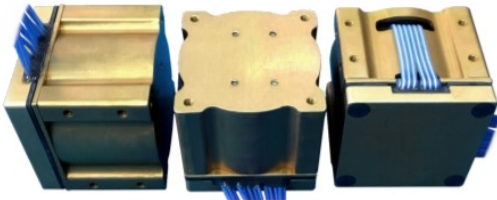


Figure 5.7: CubeSpace reaction wheels

Parameters	Requirements
T_{max}	$1.81 \text{ mN} \cdot m$
Power [W]	$< 4 \text{ W}$
Mass [kg]	$< 0.4 \text{ kg}$
Volume	$< 0.6 \text{ U}$

Table 5.7: Reaction wheels requirements

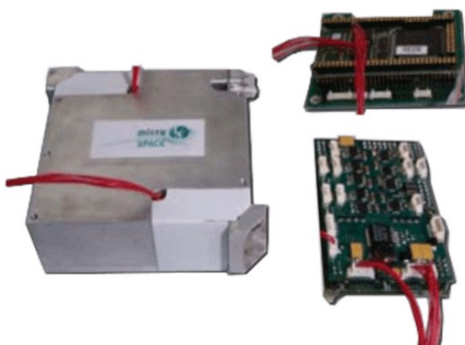


Figure 5.8: MicroSpace micro-propulsion thrusters

Parameters	Requirements
F_{max}	10 mN
Power [W]	$< 2 \text{ W}$
Mass [kg]	$< 0.4 \text{ kg}$
Volume	$< 0.5 \text{ U}$

Table 5.8: Thrusters requirements

Concerning the sensors, a configuration with 6 sun sensors and 2 star trackers have been chosen due to pointing requirements of both camera (0.01°) and HGA (0.1°). The accuracy needed shall be at least an order of magnitude below the one needed for the camera/HGA.

Hence, for star trackers the accuracy shall be in the order of 1 or 2 arcsec, while for sun sensors it shall be at least $< 0.1^\circ$. The mass of the sensors shall be minimised while retaining the desired accuracy.

CHAPTER 6

Configuration

The preliminary configuration of the spacecraft is represented in Figure 6.1 and Figure 6.2. The main driver behind this configuration is the size of the tanks required to achieve the impulsive manoeuvre at the arrival, which takes up most of the available volume of 24 U. For this reason the shape and position of some components is not ideal. Improvements in the trajectory or in the engine performance could lead to a reduction of the fuel required, allowing for a more effective arrangement.

The proposed configuration aims to fulfill the following requirements:

- The s/c shall fit inside a 24 U envelope (before deployment of appendages)
- All the deployable systems shall be able to unfold without interference: HGA, Solar Panels, TAGSAM
- The HGA reflector shall not cover the solar panels once deployed
- The HGA shall point perpendicularly with respect to the normal to the SP surface
- The TAGSAM shall be able to introduce the collected sample inside the bioreactor
- Lidar and camera shall point towards ground during the TAG phase for proximity navigation
- Engine nozzle shall point towards ground during the TAG phase to lift off after sample collection
- Camera and lidar shall be shielded from engine exhaust
- Engine nozzle shall be aligned with s/c center of mass
- Solar panels shall be mounted on the largest faces of the s/c in order to maximise their surface and minimise the hinges

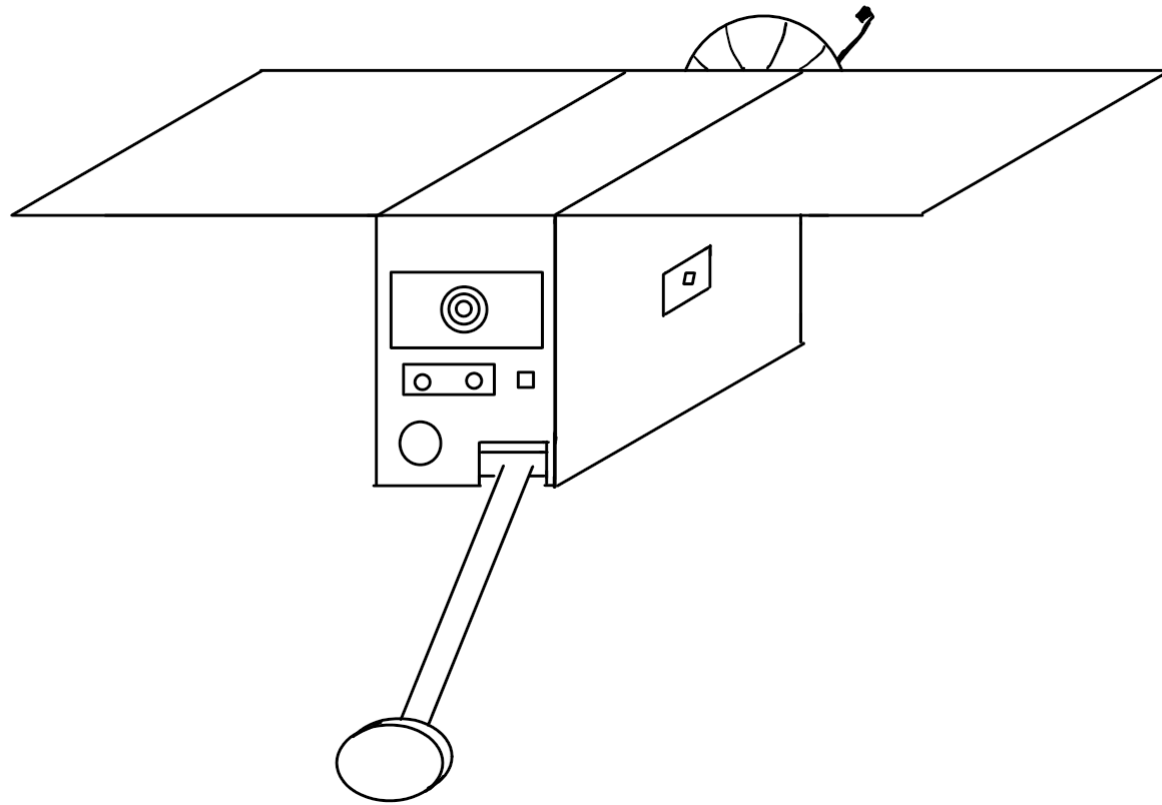


Figure 6.1: Preliminary s/c configuration



Figure 6.2: Preliminary s/c configuration breakdown

CHAPTER 7

Conclusions

From the technological point of view the mission is not ready yet, as many subsystems and payload components need further development and/or testing. In particular, the following criticalities must be highlighted:

- Methane detector: the proposed technology is at TRL 3 and the sensor needs to be interfaced with the bioreactor in order to get measurements
- TAGSAM: although the technology has been used in the OSIRIS-REx mission, it is not an "off the shelf" system and needs to be engineered and custom-built to fit inside the smallsat
- Antenna (TMTC): the HGA needs a dramatic mass reduction (from the actual 1.4 kg to 0.8 kg). Since the HGA is a mission-critical component, testing shall be performed to prevent failures
- Engine (PS): the engine base technology is ready (TRL 8, Hydros-C1), but still with not high enough specific impulse. A performance boost can be achieved according to laboratory experiments. TRL 3
- ADCS: mass reduction is required
- Structure: due to the peculiar functional requirements of the mission, the structure cannot be made using standard cubesat assemblies

Despite an apparent unfeasibility, every critical component can be actually ready in mere years. Using as approximation the one that 1 TRL step corresponds to 2 years of development, the mission could take place after 2032.

From the architecture standpoint, a more sophisticated analysis could lead to a more efficient interplanetary trajectory and a drastic reduction in the cost of the manoeuvres. This would bring several benefits, the most relevant concerning the reduction of the necessary fuel and the consequent slackening of the size and weight requirements of other components.

The mission as it has been proposed would prove to be very expensive, mainly because of the assumption that the launcher has to provide exactly the required state vector to escape Earth and begin the interplanetary travel. Since the fundamental requirement of the target body is that it must be a C-type asteroid, the mission could be redesigned to share the launch with some mothership bound for the deep space and to target a different carbonaceous asteroid. This option would allow to fulfill the primary objective, but the secondary ones would have to

be dropped. The departure of the mothership would have to be late enough to allow for all the systems and payloads to be ready.

Appendix

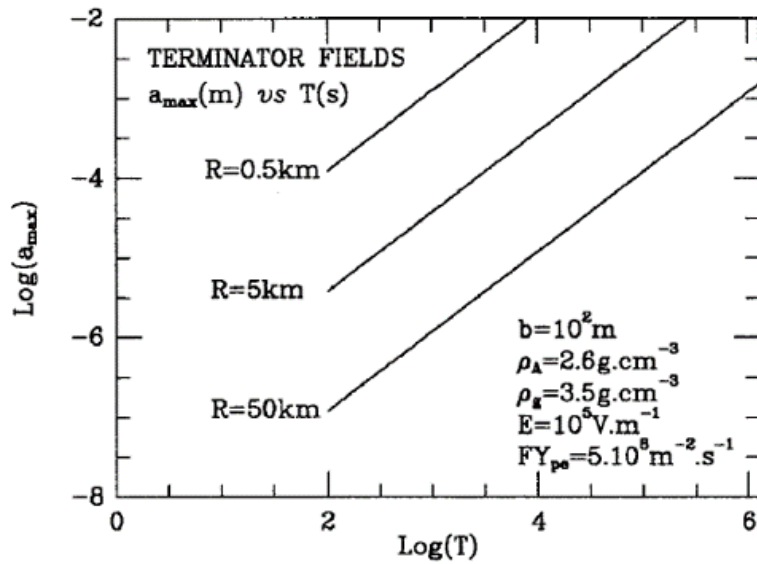


Figure 1: Radius of largest grain, a , levitable by terminator fields vs asteroid spin period, T , for various asteroid radii, R (Lee (1996))

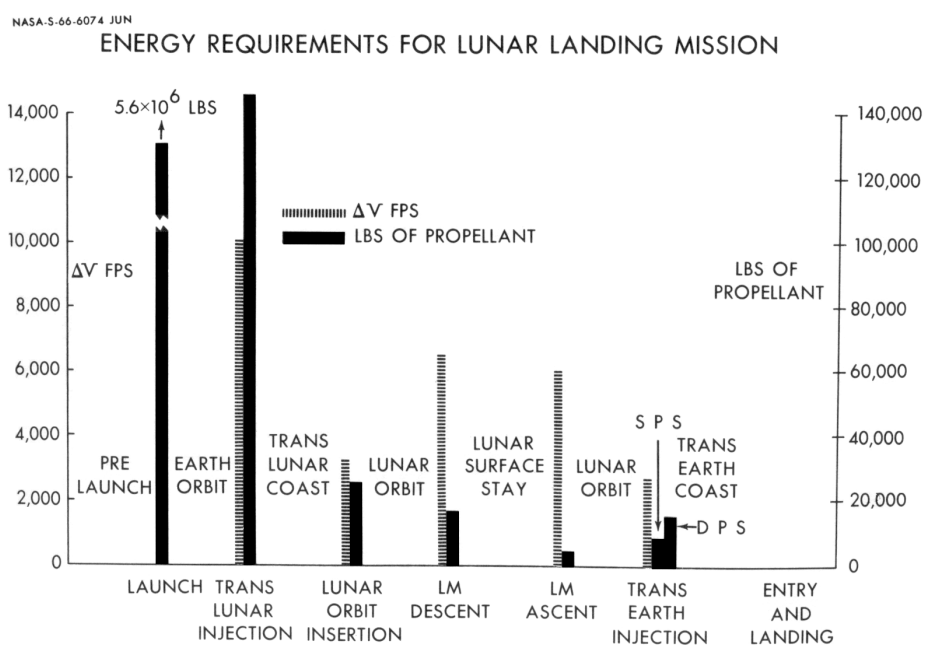


Fig. 2

Figure 2: Apollo energy requirements (Owen E. Maynard (1966))

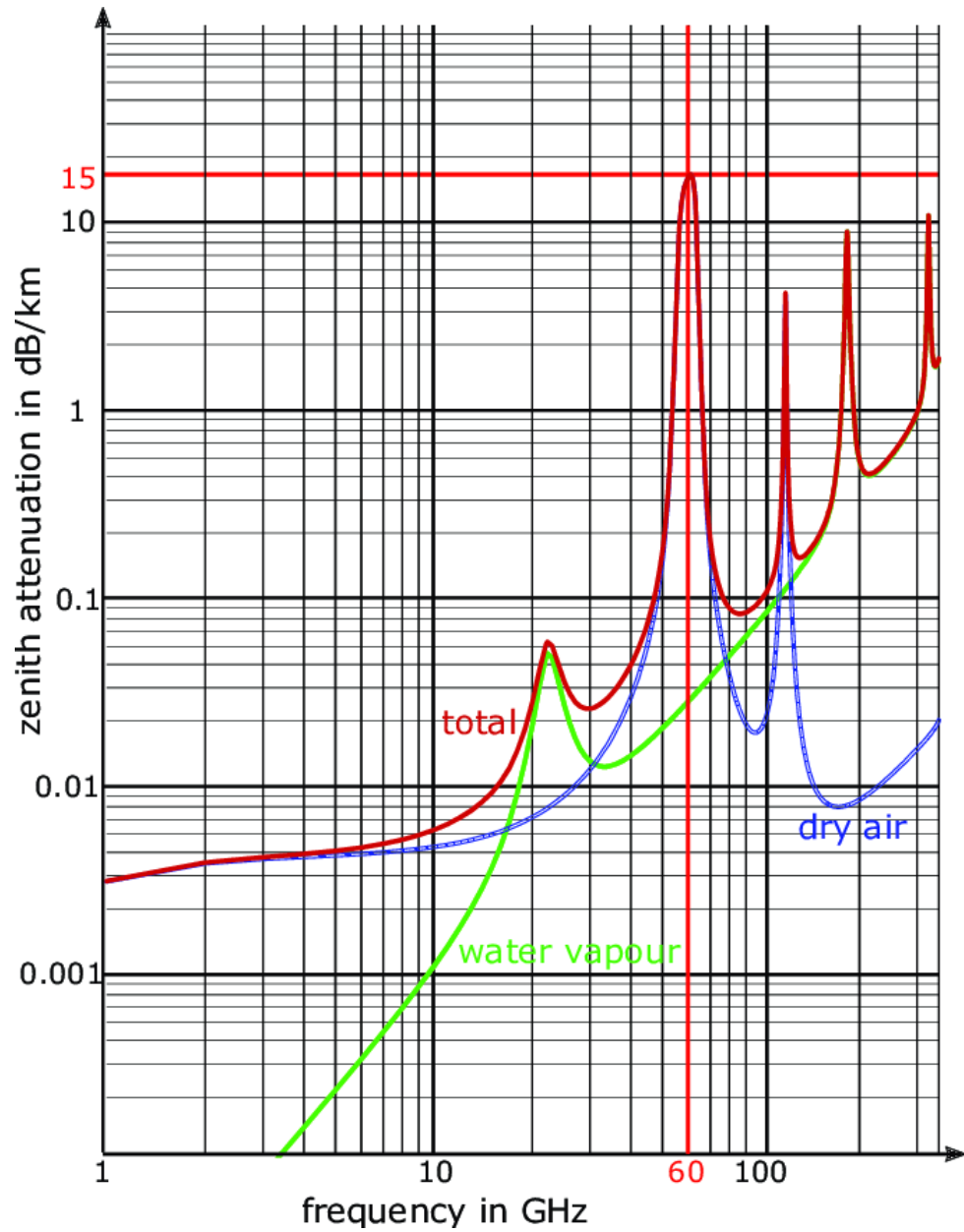


Figure 3: Atmospheric Losses (Zöchmann (2019))

Bibliography

- Aldhafeeri, T., Tran, M.-K., Vrolyk, R., Pope, M., and Fowler, M. (2020). A review of methane gas detection sensors: Recent developments and future perspectives. *Inventions*, 5(3):28. 19
- Bierhaus, E., Clark, B., Harris, J., Payne, K., Dubisher, R., Wurts, D., Hund, R., Kuhns, R., Linn, T., Wood, J., et al. (2018). The osiris-rex spacecraft and the touch-and-go sample acquisition mechanism (tagsam). *Space Science Reviews*, 214(7):1–46. 23
- Cavicchioli, R. (2002). Extremophiles and the search for extraterrestrial life. *Astrobiology*, 2(3):281–292. 18
- Chahat, N., Hodges, R. E., Sauder, J., Thomson, M., Peral, E., and Rahmat-Samii, Y. (2016). Cubesat deployable ka-band mesh reflector antenna development for earth science missions. *IEEE Transactions on Antennas and Propagation*, 64(6):2083–2093. 33
- Cockell, C. S., Santomartino, R., Finster, K., Waajen, A. C., Eades, L. J., Moeller, R., Rettberg, P., Fuchs, F. M., Van Houdt, R., Leys, N., et al. (2020). Space station biomining experiment demonstrates rare earth element extraction in microgravity and mars gravity. *Nature communications*, 11(1):1–11. 19
- Elshurafa, A. M. and Aldubyan, M. H. (2019). State-of-charge effects on standalone solar-storage systems in hot climates: A case study in saudi arabia. *Sustainability*, 11:3471. 29
- Goldberg, H. R., Karatekin, Ö., Ritter, B., Herique, A., Tortora, P., Prioroc, C., Gutierrez, B. G., Martino, P., and Carnelli, I. (2019). The juventas cubesat in support of esa’s hera mission to the asteroid didymos. 22
- Hodges, R. E., Chahat, N., Hoppe, D. J., and Vacchione, J. D. (2017). A deployable high-gain antenna bound for mars: Developing a new folded-panel reflectarray for the first cubesat mission to mars. *IEEE Antennas and Propagation Magazine*, 59(2):39–49. 33
- Klas, M., Tsafnat, N., Dennerley, J., Beckmann, S., Osborne, B., Dempster, A. G., and Manefield, M. (2015). Biomining and methanogenesis for resource extraction from asteroids. *Space Policy*, 34:18–22. 18
- Kohout, T., Näsilä, A., Tikka, T., Granvik, M., Kestilä, A., Penttilä, A., Kuhno, J., Muinonen, K., and Viherkanto, K. (2017). Asteroid spectral imaging mission (aspect) cubesat to characterize resources on asteroid surfaces. In *European Planetary Science Congress*, pages EPSC2017–496. 21
- Larson, H. P., Feierberg, M. A., Fink, U., and Smith, H. A. (1979). Remote spectroscopic identification of carbonaceous chondrite mineralogies: Applications to ceres and pallas. *Icarus*, 39(2):257–271. 21
- Lee, P. (1996). Dust levitation on asteroids. 6, 41

- Mauerhofer, L.-M., Zwirtmayr, S., Pappenreiter, P., Bernacchi, S., Seifert, A. H., Reischl, B., Schmider, T., Taubner, R.-S., Paulik, C., and Simon, K.-M. R. (2021). Hyperthermophilic methanogenic archaea act as high-pressure ch 4 cell factories. *Communications biology*, 4(1):1–12. 19
- May, A., Sutter, B., Linn, T., Bierhaus, B., Berry, K., and Mink, R. (2014). Osiris-rex touch-and-go (tag) mission design for asteroid sample collection. 15
- Owen E. Maynard, J. R. S. (1966). *Apollo Lunar Landing Mission Symposium, Manned Spacecraft*. 15, 41
- Peral, E., Statham, S., Im, E., Tanelli, S., Imken, T., Price, D., Sauder, J., Chahat, N., and Williams, A. (2018). The radar-in-a-cubesat (raincube) and measurement results. In *IGARSS 2018-2018 IEEE International Geoscience and Remote Sensing Symposium*, pages 6297–6300. IEEE. 33
- Pothamsetti, R. and Thangavelautham, J. (2016). Photovoltaic electrolysis propulsion system for interplanetary cubesats. In *2016 IEEE Aerospace Conference*, pages 1–10. IEEE. 25
- Triki, M., Ba, T. N., and Vicet, A. (2015). Compact sensor for methane detection in the mid infrared region based on quartz enhanced photoacoustic spectroscopy. *Infrared Physics & Technology*, 69:74–80. 20
- Vercoutere, W., Navarro, B. J., Rask, J., and Krause, A. (2008). Space faring: The radiation challenge. 6
- Wilkinson, J. (2009). *Probing the new solar system*. 6
- Zöchmann, E. (2019). *On the occurrence of two-wave with diffuse power fading in millimeter wave communications*. PhD thesis, Wien. 42